J Mater Sci: Mater Electron (2015) 26:7165–7173
DOI 10.1007/s10854-015-3341-4

Effect of titanyl phthalocyanine doping on opto-electrical properties of Alq_3 thin films

M. Ramar[1,2] · V. Yadav[1,2] · R. Srivastava[2] · C. K. Suman[2]

Received: 15 March 2015 / Accepted: 6 June 2015 / Published online: 13 June 2015

Abstract The titanyl phthalocyanine (TiOPc) was doped in tris (8-hydroxy quinolinato) aluminum (Alq_3) with concentration of 1, 2 and 3 % by weight. The thin film of undoped and doped Alq_3 was studied extensively for optical and electrical properties. The refractive index of the studied material was found in the range of 1.5–2.07 for 300–1000 nm wavelength. The Urbach tail energy decreases by increase of doping concentration. The PL quenching ratio increases with doping that attribute charge transfer from Alq_3 to the TioPc. The electrical properties of the thin film were studied by impedance spectroscopy over a frequency range of 100 Hz–1 MHz. The undoped and doped Alq_3 shows single relaxation process. The Cole–Cole plots of undoped and doped device can be represented by a single parallel resistance R_P and capacitance C_P network with a series resistance R_S. The value of R_P and C_P at zero bias are $\sim$146 kΩ, 87 kΩ, 814 Ω and 22 kΩ and 68, 9, 30 and 29 nF for undoped, 1, 2 and 3 % doping, respectively. The resistance R_P decreases with applied bias whereas the capacitance C_P remains almost constant. At high frequency, the AC conduction of the film follows the universal power law and the onset frequency increases with increasing bias voltages.

✉ C. K. Suman
sumanck@nplindia.org

[1] Academy of Scientific and Innovative Research (AcSIR), CSIR-National Physical Laboratory Campus, Dr. K. S. Krishnan Marg, New Delhi 110012, India

[2] CSIR-Network of Institutes for Solar Energy, CSIR-National Physical Laboratory Campus, Dr. K. S. Krishnan Marg, New Delhi 110012, India

1 Introduction

Recently, organic semiconductors have become very attractive materials capable of replacing inorganic semiconductors in the development of low-cost, large area and light weight optoelectronic devices, such as organic light emitting diodes (OLEDs), organic solar cells (OSCs) and organic thin film transistors (OTFTs) [1–5]. The doping in organic semiconductor plays a vital role in tuning the optical and electrical properties [6, 7]. The interface between organic semiconductors and metals are also dependent on the doping concentration. The carrier injection in the device is influenced by suitable dopant in the organic semiconductor that leads to the enhancement of device life time [8, 9]. Now a days, there is a new trend in doping of organic semiconductor for reducing the contact resistance with metal and lowering the energy barrier at the interface due to band bending [10, 11]. The metal contacts determine the energy barrier to injection of electrons and holes. Thus, the choice of metal contacts determines whether the device is electron only, hole only or bipolar. Metals with small work functions such as Ca or Sm give a small barrier to injection of electrons and high work function metals such as Pt or Au give a small barrier for injection of holes. Similarly Aluminium (Al) gives a large barrier for injection of holes into Alq_3 thin films. The electrical properties of single carrier device are influenced by either injection at contacts or by space charge in the organic thin film [12, 13].

However; the opto-electrical properties of organic materials have been widely investigated and those properties have been exploited for efficient device application. But due to large number of doping material (like carbonate, fluoride and oxide group material) and their complexity;

the opto-electrical properties of doped organic semiconductor needs more research focus.

In this work we have discussed about the optical and electrical properties of TiOPc doped Alq_3 thin films using Ellipsometry, Absorption, PL and impedance spectroscopy (IS) in the broad frequency range 100 Hz–1 MHz.

2 Experimental methods

The co-evaporation process was used for TiOPc doping in Alq_3. The undoped Alq_3, 1, 2 and 3 % by weight doping concentration thin film and related electron only devices (EOD) were named as A, B, C and D. The EOD were fabricated on glass substrates in the structure of Al/organic/Al. The EOD is fabricated of a 100 nm thick undoped and doped Alq_3 with same 100 nm Al as both electrode. Before loading into evaporation chamber for device and thin film fabrication, glass substrates were subjected to a routine cleaning process ultrasonically cleaned with de-ionized water, acetone and isopropyl alcohol and finally dried the substrates. All the organic and metal layers were sequentially thermally deposited on top of the substrates in a high vacuum deposition system with a base pressure of $\sim 10^{-6}$ Torr through shadow masks, while the deposition rate was kept to be 1–2 A°/s for organic layers and 2–5 A°/s for metal electrode. The overlap of Al electrode defines the active area of the device to be 9 mm^2.

The optical properties of the thin film was measured by Ellipsometry (J.A.Woolam-M2000), UV–Vis Spectrometer and PL setup (Horiba). A IS measurement was performed using Impedance/Gain-Phase Analyzer (Solartron, model SI 1260) System. A 100 mV amplitude AC signal superimposed on a DC bias was used to measure the device Impedance as a function of AC frequency and DC bias.

3 Results and discussion

Tris (8-hydroxy quinoline) aluminum (Alq_3) are widely used organic semiconductor as an electron transport or light emitting layer in OLEDs. The Alq_3 chemical structure have two possible geometrical isomers of Alq_3, meridional (C_1 symmetry) and facial (C_3 symmetry) forms. In the meridional isomer, the three ligands are not equivalent with respect to the Al atom, while they are equivalent in the facial isomer. Generally; the meridional isomer is the dominant species in most cases, such as in amorphous and crystalline states. The meridional isomer is more stable than the facial isomer. Figure 1a shows schematic energy diagrams and Fig. 1b shows the device architecture. The device contains the vertical stacking of metal electrode aluminum both side and doped active material thin films in

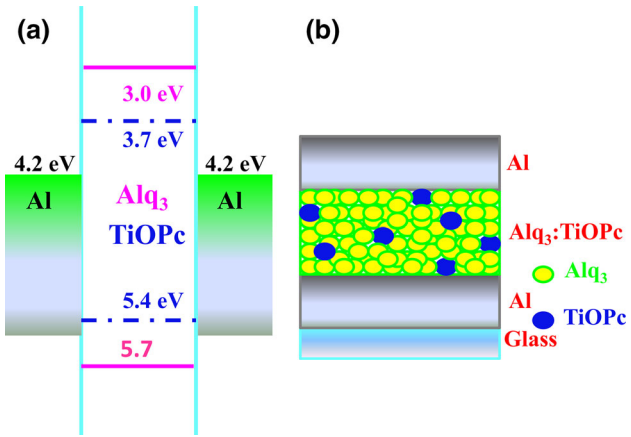

Fig. 1 **a**, **b** The schematic energy diagrams and the device architecture

the center. The highest occupied molecular orbital (HOMO)–lowest unoccupied molecular orbital (LUMO) values of Alq_3 and TiOPc are 5.7–3.0 and 5.4–3.7 eV respectively. The LUMO and HOMO level of TiOPc is located between the LUMO and HOMO of Alq_3, respectively.

3.1 Optical properties

The ellipsometric response of the thin film was measured in the 200–1000 nm spectral range at an incident angle of 50°. The refractive index (n) and extinction coefficient (k) spectra are shown in Fig. 2a, b for undoped and doped Alq_3. The index of refraction is found between 1.5 and 2.07 in the whole wavelength ranges. These n values are higher than the typical organic semiconductor used as electron transport layer. As shown in Fig. 2b, the doped Alq_3 film has a lower extinction coefficient (k) in the spectral range between wavelengths of $\lambda = 360$ and 450 nm, compared to that undoped Alq_3. Anisotropic materials typically have at least two different optical constants: Ordinary optical constants for p-polarized light and extraordinary optical constants for s-polarizations. The ordinary extinction coefficient for the planar molecule is larger than the extraordinary coefficient, and hence the absorption of molecules depends on its preferred orientation in the film, which in turn is strongly affected by the substrate and growth process [14]. In our case, we attribute the decreased extinction coefficient in doped films to a preferred molecular orientation along the axis of lower k relative to the light that is incident normal to the substrate. Hence, we conclude that the nanocrystalline morphology of TioPc affects the orientation of the Alq_3 thin film whereas this preferred orientation is not observed in undoped Alq_3 thin film.

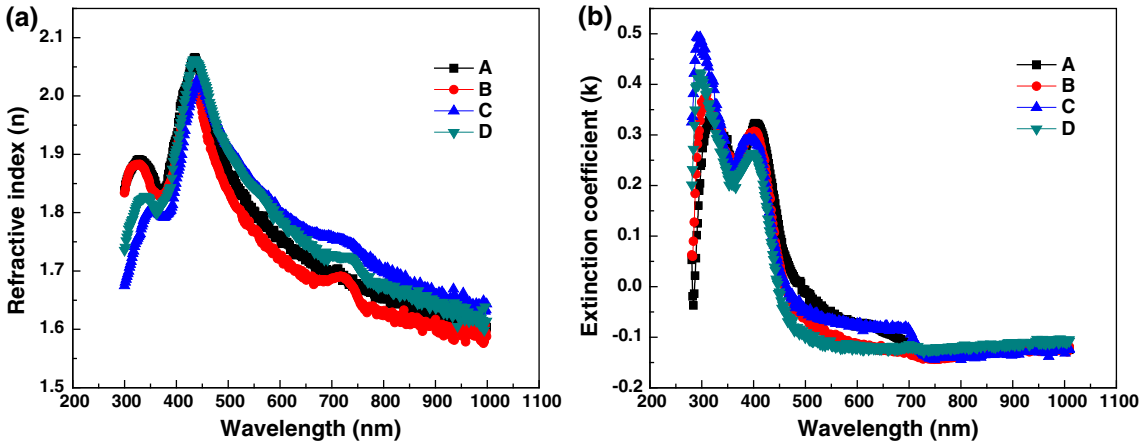

Fig. 2 **a** Refractive index (n) and **b** extinction coefficient (k) as a function of wavelength

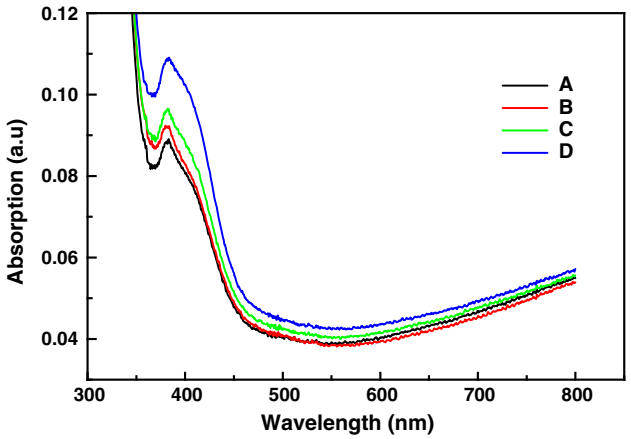

Fig. 3 Absorption spectra of thin film *A*, *B*, *C* and *D* for wavelength 300–800 nm

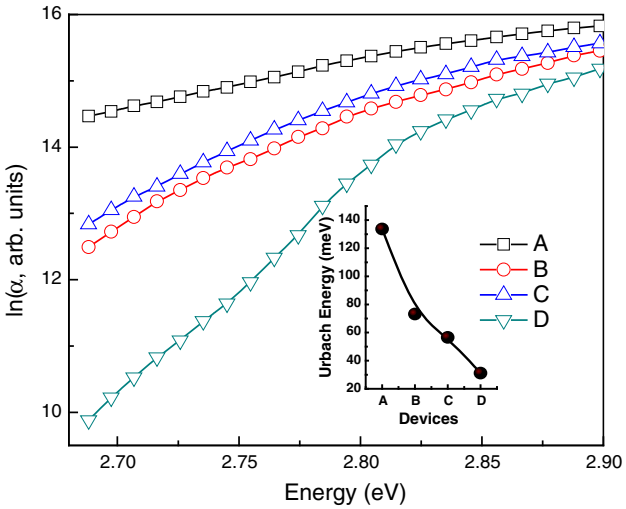

Fig. 4 The variation of absorption coefficient with energy. *Inset figure*—the change of Urbach tail energy with doping concentration

Figure 3 shows the absorption spectrum in the wavelength range 200–1000 nm. The maximum absorption in undoped and doped Alq_3 thin film was observed at a wavelength of 387 nm. No absorption peak was observed for TiOPc material in the doped thin film. This may be due to low concentration of doping. There is no shift in the peak of the doped Alq_3 which corresponds to no change in optical band gap with doping.

Figure 4 Shows the natural logarithm of the absorption coefficient (log(α)) of undoped and doped Alq_3 thin film versus energy near the film long wavelength cutoff. Since the nanostructure of the organic film affects the allowed optical transitions near the HOMO–LUMO energy gap (i.e. near the long wavelength optical cutoff), [15, 16]. We can analyze the spectral properties of the films in this region to gain further information about their morphologies. That is, structural disorder leads to a broadened density of states that result in an Urbach tail near the absorption cutoff [17–19] that follows

$$\alpha = \alpha_0 \exp(hc/\lambda U) \tag{1}$$

here, α_0 is a constant, h is Planck's constant, c is the speed of light, and U is the Urbach tail energy. The Urbach tail energies for A to D thin film was found to be 133.6 meV, 73.2, 56.5 and 31.1 meV, respectively. The doping of Alq_3 with TioPc decreases the Urbach tail energy (shown in inset of Fig. 4). This decrease in Urbach tail energy attributes to increase of structural disorder with doping concentration.

Figure 5 shows the PL spectrum in the wavelength range of 200–1000 nm. The photo-luminescence intensity (PL) peak was observed at 517 nm on undoped and doped Alq_3 thin film. The wavelength of maximum peak value is not change, but only intensity of PL quenching reduced. We calculated the PL quenching ratio Φ according to:

$$\varphi = \int PL_{Alq3}(\lambda)d\lambda \Big/ \int PL_{Alq3:TiOPc}(\lambda)d\lambda \tag{2}$$

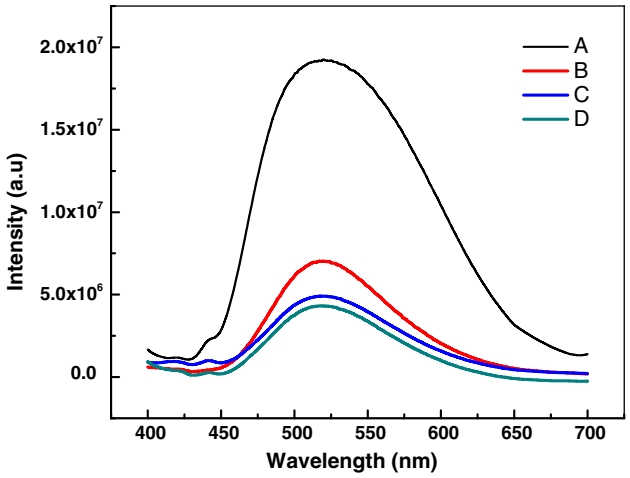

Fig. 5 Photoluminescence (PL) intensity spectra of TiOPc doped Alq_3 thin film

where $PL_{Alq3}(\lambda)$ and $PL_{Alq3:TioPc}$ (λ) describe the PL spectrum of neat Alq_3 and the Alq_3:TioPc composite, respectively. Our measurements revealed that in Alq_3:-TioPc films the Alq_3 emission is strongly quenched as evidenced by a large PL quenching ratio Φ for 1, 2 and 3 % doping $\sim$37, 42 and 51, respectively. The quenching ratio indicates good charge transfer from Alq_3 to the TioPc. Thus, we conclude that Alq_3:TiOPc doped thin film are finely mixed. [20]

3.2 Electrical properties

Figures 6 and 7 Show the frequency dependence of the real (Re Z) and imaginary (Im Z) parts of impedance at different bias voltages. The complex impedance $Z(f)$, can be represented as a function of frequency as,

$$Z(f) = Z'(f) + Z''(f) \tag{3}$$

where Z' and Z'' are the real and imaginary parts of impedance. It is observed that the magnitude of Re Z are constant with frequency up to 95, 310, 10 k and 384 Hz in device A, B, C and D respectively and it decreases with frequency between 95 Hz–1.5 kHz, 310 Hz–10 kHz, 10 kHz–1 MHz and 384 Hz–10.2 kHz in device A, B, C and D respectively. The magnitude of Re Z decreases with applied bias voltages but for all voltage the value of Re Z merges in the higher frequency. All the four A, B, C and D thin film show single relaxation process and indicate an increase in ac conductivity with frequency. The ImZ reaches a maximum peak $Im(Z)_{max}$ for all bias voltage at different frequency. The frequency corresponding to $Im(Z)_{max}$ called relaxation frequency shifts to higher values with increase of applied bias voltage. This is an indication

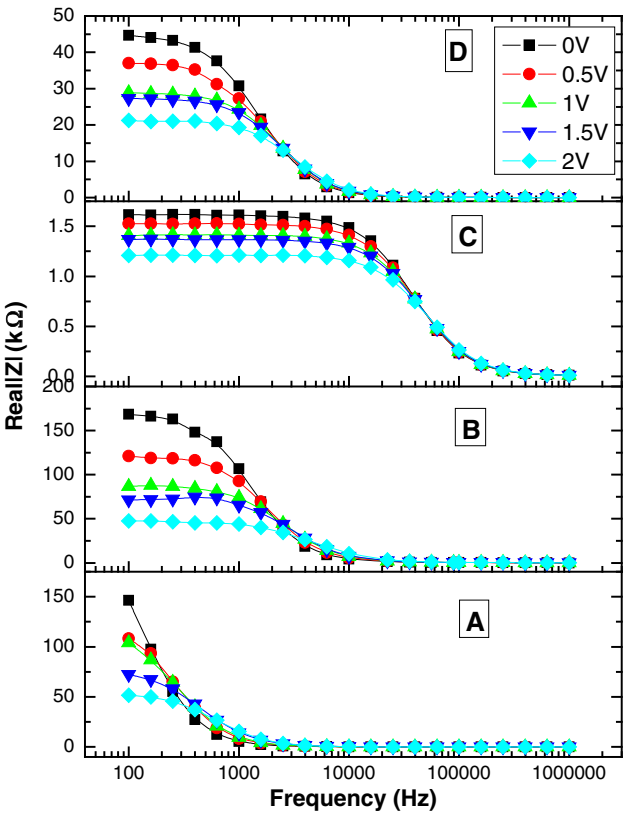

Fig. 6 Real part of impedance as a function of frequency at various applied bias voltages for devices *A*, *B*, *C* and *D*

of increasing loss in the materials with increase of applied bias voltage.

The peak heights are proportional to bulk resistance (R_b) [21] according to equation

$$Z'' = R_b[\omega\tau/(1+\omega^2\tau^2)], \tag{4}$$

in Z'' versus frequency plots. At the peak the relaxation is defined by the condition $\omega_m\tau_m = 1$ where τ_m is the relaxation time. It has been clearly observed that the relaxation frequency shifts to higher side by TioPc doping up to 2 % concentration, resulting in lowering of relaxation time. In hopping conduction the relaxation frequency [22] is given by

$$\omega_m = \omega_0 \exp(-E_a/K_BT), \tag{5}$$

where ω_0 is the phonon frequency usually in the range of 10^{12}–10^{13} Hz and E_a is the activation energy. The activation energy estimated for undoped Alq_3, 1, 2 and 3 % TiOPc-doped Alq_3 are 0.23, 0.21, 0.17 and 0.20 eV, respectively. The Cole–Cole plots of the Re Z and Im Z at 100 Hz–1 MHz for different dc bias voltages at room temperature for the device are shown in Fig. 8. The plot shows a single semicircle at bias voltages 0–2 V and the size of the semicircle decreases rapidly as the dc bias

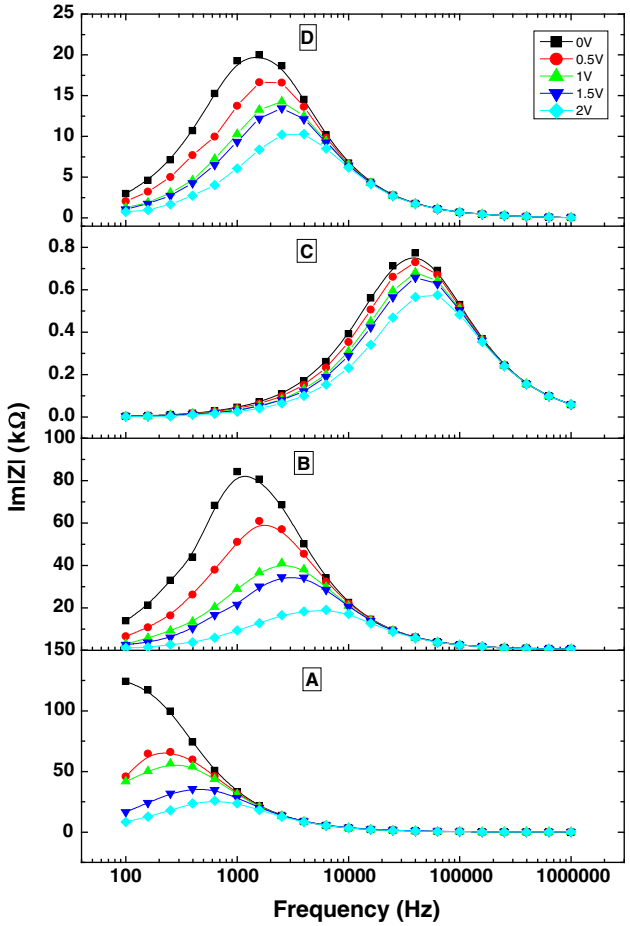

Fig. 7 Imaginary part of impedance as a function of frequency at various applied bias voltages for devices *A*, *B*, *C* and *D*

voltage increases. Therefore, all devices (A, B, C, and D) can be modeled as an RC equivalent electrical circuit of which a contact series resistance R_S with a single parallel resistance (R_P) and the capacitance (C_P) network. The impedance of the RC equivalent electrical circuit (using Eqs. 3 and 4) can be giving by [23].

$$Z = \mathrm{Re}Z + \mathrm{Im}Z = \left[R_S + \frac{R_P}{1+\omega^2 R_P^2 C_P^2}\right] - i\left[\frac{\omega R_P^2 C_P}{1+\omega^2 R_P^2 C_P^2}\right] \quad (6)$$

By eliminating the angular frequency, the semicircle of the Cole–Cole plot can be written as

$$\left[\mathrm{Re}Z - \left(R_S + \frac{R_P}{2}\right)\right]^2 + (-\mathrm{Im}Z)^2 = \left(\frac{R_P}{2}\right)^2 \quad (7)$$

This relation defines a circle centered at ($R_S + R_P/2$, 0) with radius of $R_P/2$. The minimum Re Z value represents the value of R_S with the capacitance and it is about 60 Ω in all devices and almost same for different applied bias voltage. The R_S can be considered as originating from the electrode contact. The maximum Re Z value corresponds to the summation of R_S and R_P to the capacitance. In Fig. 8 the symbols are the experimental values and the solid lines are the theoretical results obtained from Eq. (7). There is perfect agreement between the experimental and theoretical impedance results.

The fitting data based on Eq. (6) are shown in Fig. 9. It can be seen that the C_P is almost independent on the bias voltage, but the R_P decreases as the applied bias voltage increases. Generally, C_P is directly related to the intrinsic property of used materials. The independence of C_P on the bias voltage indicates that the device should be acted as a simple parallel plate capacitor. The decrease of R_P with bias voltage is due to a large number of injected electrons. This also indicates that the effective conductivity of the organic material will increase with the bias voltage. The value of Rp and Cp for A, B, C and D devices are ~146 kΩ, 87 kΩ, 814 Ω, 22 kΩ and 68, 9, 30, 29 nF, respectively.

The ac electrical conductivity was obtained by the relation

$$\sigma_{ac} = \frac{l}{AZ'} \quad (8)$$

where l is the thickness of sample, A is the area and Z is the impedance. Figure 10 shows the variation of ac conductivity with frequency at different bias voltages. It is clear that the ac conductivity increases with increasing frequency. For all the voltages, there are two different regions in the ac conductivity, the frequency independent and dependent region at low and high frequency region. The onset (switch from frequency-independent to frequency-dependent region) shifts towards higher side with applied bias voltages. The frequency dependent region display a power law dependence as predicted for conducting materials by Jonscher [24].

$$\sigma_{ac} = \sigma_{dc} + A\omega^s \quad (9)$$

where σ_{dc} is the frequency-independent conductivity, ω is the angular frequency of the applied AC electric field in the frequency sensitive region, A and s ($0 \leq s \leq 1$) are material and doping dependent constants. It is found that the value of s decreases with applied bias voltage increases as shown in Fig. 11. In order to explain the behavior of σ_{ac} with frequency and temperature, different theoretical models have been proposed to correlate the conduction mechanism of ac conductivity with frequency exponent s. Various theoretical models proposed for ac conduction in amorphous semiconductors are quantum mechanical tunneling (QMT), classical hopping over barrier (HOB) and correlated barrier hopping (CBH). QMT model refers to the carrier motion that occurs through tunneling between two localized states near the Fermi level. In CBH model, two electrons or holes simultaneously hop over the potential barrier between two charged defect states (bipolaron

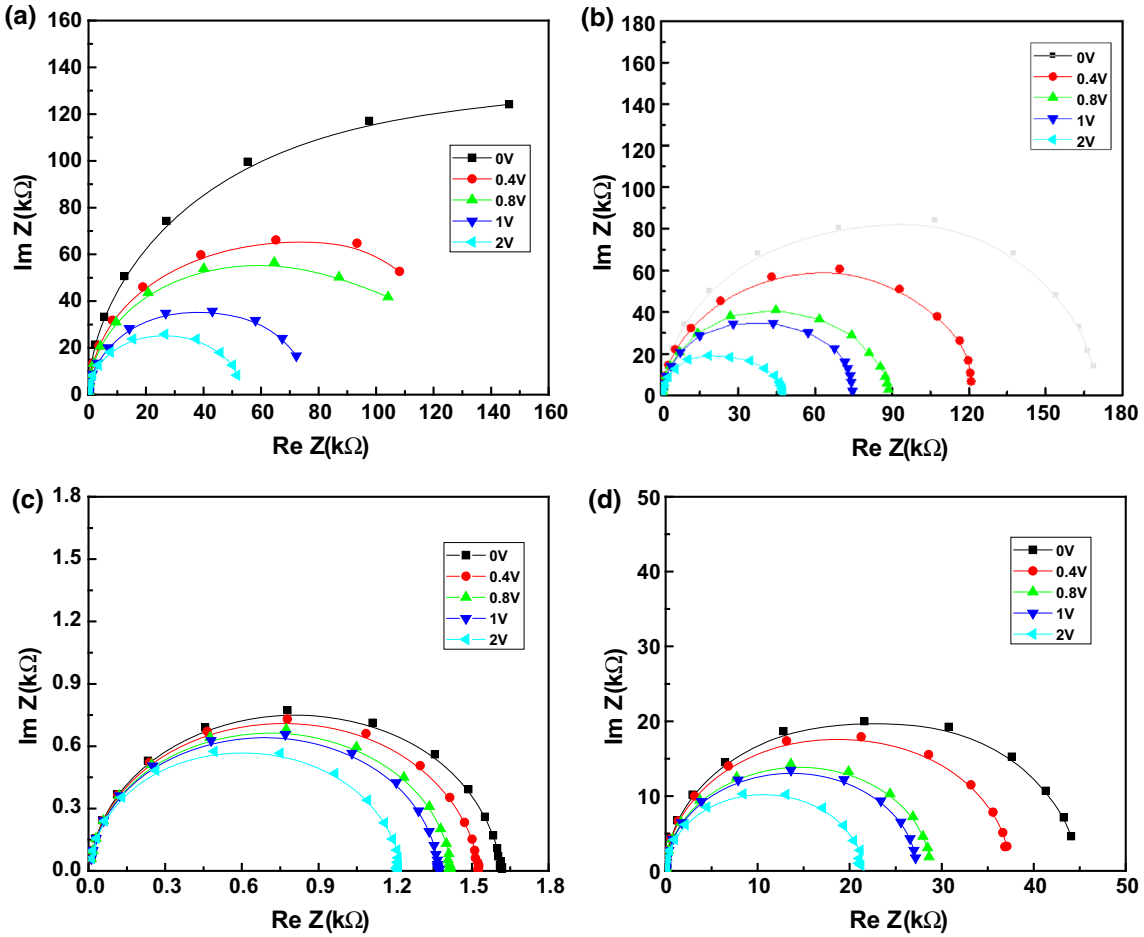

Fig. 8 Cole–Cole plots at different bias voltages at room temperature of devices A, B, C and D

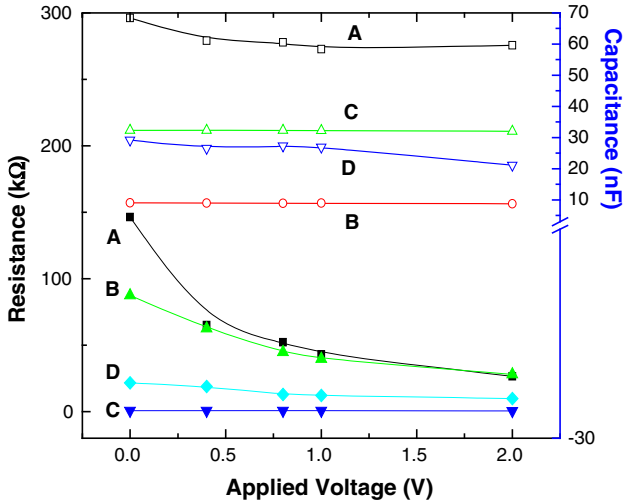

Fig. 9 The variation of bulk resistance R_P and capacitance C_P with different applied bias voltages for devices A, B, C and D

hopping) and the barrier height W is correlated with the intersite separation, R, via Coulombic interaction. Barrier height, W is given by

$$W = W_M - {ne^2}/{\pi\varepsilon\varepsilon_0 R} \tag{10}$$

where W_M is maximum barrier height, n is the number of electrons involved in the hoping process, n = 1 for single polaron hopping and n = 2 for bipolaron hopping, e is an electronic charge, ε and ε_o are the dielectric constants of material and free space, respectively.

The ac conductivity can be evaluated for this mechanism as [25]

$$\left.\begin{aligned} \sigma_{ac} &= \frac{n\pi^3}{24} N^2 \varepsilon\varepsilon_o R_\omega^6 \\ R_\omega &= \frac{ne^2}{\pi\varepsilon\varepsilon_o [W_M + KT\ \ln(\omega\tau_o)]} \end{aligned}\right\} \tag{11}$$

where N is the concentration of pair states and Rω is the hopping distance at a frequency ω

The frequency exponent for this model can be evaluated as

$$S = 1 - \frac{6KT}{W_M + KT\ \ln(\omega\tau_0)} \tag{12}$$

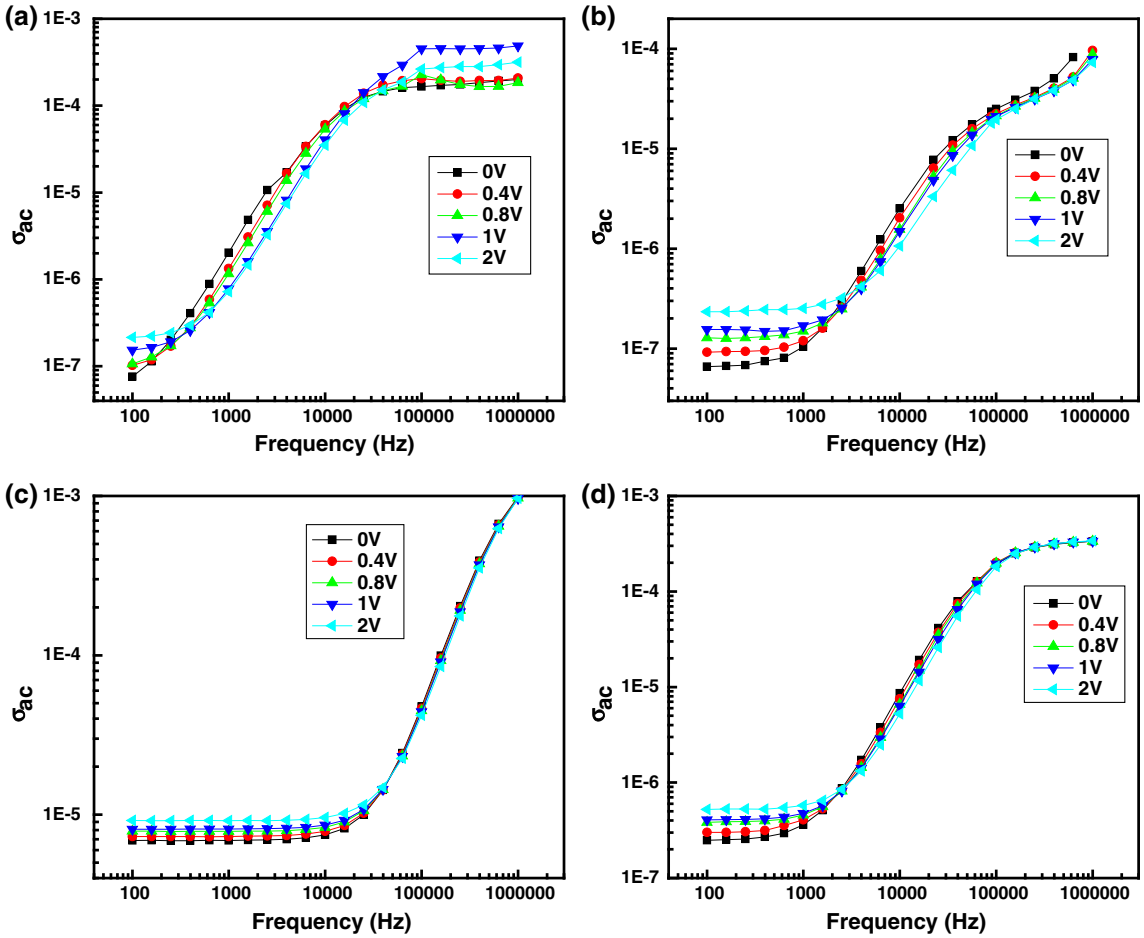

Fig. 10 The ac conductivity of device at various applied bias voltages of devices *A*, *B*, *C* and *D*

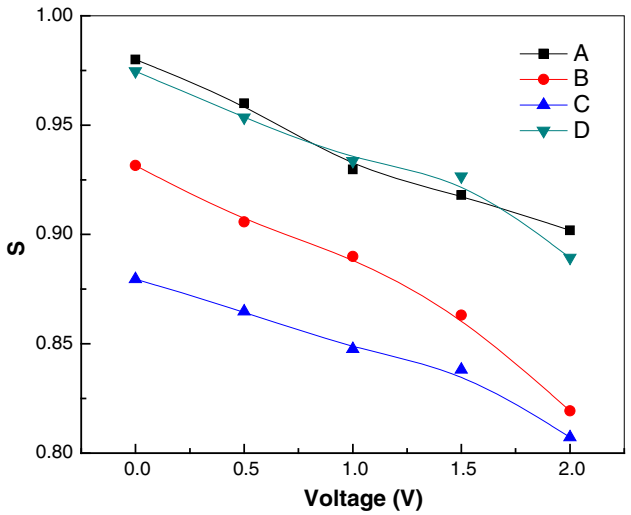

Fig. 11 The variation of s with applied bias voltages for device *A*, *B*, *C* and *D*

Figure 12a–c shows the calculated minimum hopping distance, the binding energy W_M and density of states $N(E_f)$ for undoped and doped thin film. The hopping distance and density of states increases with doping up to 2 % and for more doping concentration it starts decreasing whereas the binding energy has completely reverse trend of hoping distance. The binding energy decreases with doping up to 2 % concentration and starts increasing for higher doping. The binding energy decreases with increasing the bias voltage for all the devices and the hopping distance increases with bias but the effect of bias is very low on both the hopping distance as well as on binding energy. The estimated density of states value at Fermi level (at 100 kHz) for all the devices A, B, C and D are 9×10^{22}, 11×10^{22},18×10^{22} and 45×10^{22} eV^{-1} cm^{-3}, respectively. The density of states near the Fermi level is dominated by doping, impurities, decomposition or the different molecular phases and the interfacial region effect [26]. Due to the coulomb interaction between the release charge carriers and the dopant the deep tails of the intrinsically Gaussian DOS distribution broadens [27]. Hence the dopant concentration increases the total density of deep localized states. The doping of TiOPc increases the charge concentration and so the conductivity as well as the coulomb traps. The width of intrinsic DOS and the external

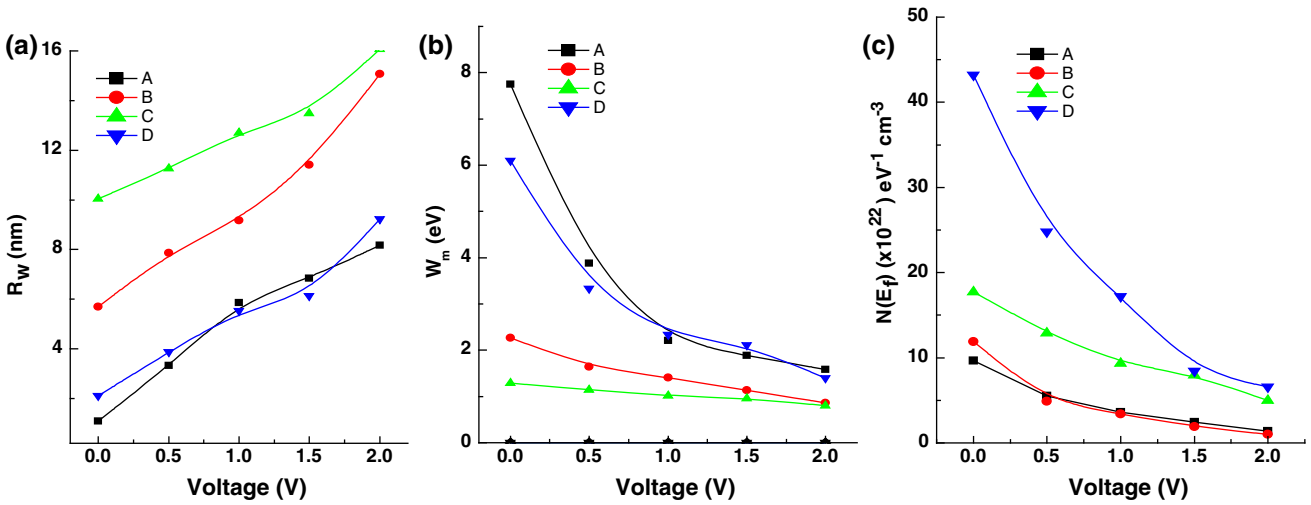

Fig. 12 **a** Voltage dependence of minimum hopping distance (R_{min}), **b** binding energy (W_{min}) and **c** density of states (N_{Ef}) at 1 kHz for *A–D* device

electric filed strength control both the increase of density of charge carriers and the coulomb traps.

4 Conclusions

The higher value of refraction index between 1.5 and 2.07 was found for undoped and doped Alq_3. Lower extinction coefficient in doped films was attributed to a preferred molecular orientation along the axis of lower *k* relative to the light. The Urbach tail energies, $U = 133.6$ meV, 73.2, 56.5 and 31.1 meV for A to D thin film was found. This decrease in Urbach tail energy indicated increase of structural disorder with doping concentration. In doped thin films; the Alq_3 emission is strongly quenched. The PL quenching ratio Φ for 1, 2 and 3 % doping are $\sim$37, 42 and 51, respectively. Thus it may be concluded that doped thin film are finely mixed. All the devices A to D can be modeled as an equivalent parallel RC network as observed by Cole–Cole plot. The R_P is highly dependent on voltage where as the C_P is independent of applied bias. The value of s decreases with applied bias voltage for all the devices. The hopping distance and density of states increases with doping up to 2 % and for more doping concentration it decreases whereas the binding energy has completely opposite trend. The estimated density of states value at Fermi level (at 100 kHz) for all the A to D devices are 9×10^{22}, 11×10^{22}, 18×10^{22} and 45×10^{22} eV^{-1} - cm^{-3}, respectively. The density of states near the Fermi level is dominated by doping, impurities, different molecular phases and the interfacial region effect. The doping of TiOPc increases the charge concentration and so the conductivity as well as the coulomb traps. The conduction is well explained by CBH model.

Acknowledgments The authors gratefully recognize the financial support from the Council of Scientific and Industrial Research (CSIR), India for funding research work.

References

1. C.W. Tang, S.A. VanSlyke, Appl. Phys. Lett. **51**, 913 (1987)
2. S.R. Forrest, Nature **428**, 911 (2004)
3. C.W. Tang, Appl. Phys. Lett. **48**, 183 (1986)
4. M. Ramar, C.K. Suman, R. Manomozhi, R. Ahamed, R. Srivastava, RSC Adv. **4**, 32651 (2014)
5. J. Huang, M. Pfeiffer, A. Werner, J. Blochwitz, K. Leo, S. Liu, Appl. Phys. Lett. **80**, 139 (2002)
6. C.-C. Chang, M.-T. Hsieh, J.-F. Chen, S.-W. Hwang, C.H. Chen, Appl. Phys. Lett. **89**, 253504 (2006)
7. X.L. Zhu, J.X. Sun, H.J. Peng, Z.G. Meng, M. Wong, H.S. Kwoka, Appl. Phys. Lett. **87**, 153508 (2005)
8. D. Grozea, A. Turak, Y. Yuan, S. Han, Z.H. Lu, W.Y. Kim, J. Appl. Phys. **101**, 033522 (2007)
9. K.L. Tang, S.W. Tsang, K.K. Tsang, S.C. Tse, S.K. So, J. Appl. Phys. **102**, 093705 (2007)
10. S.W. Tsang, Z.H. Lu, Y. Tao, Appl. Phys. Lett. **90**, 132115 (2007)
11. M.T. Hsieh, C. Chang, J.F. Chen, C.H. Chen, Appl. Phys. Lett. **89**, 103510 (2006)
12. M.A. Lampertand, P. Mark, *Current Injection in Solids* (Academic, New York, 1970)
13. B.K. Crone, I.H. Campbell, P.S. Davids, D.L. Smith, C.J. Neef, J.P. Ferraris, J. Appl. Phys. **86**, 5767 (1999)
14. D. Yokoyama, K. Nakayama, T. Otani, J. Kido, Adv. Mater. **24**, 6368 (2012)
15. M.S. Dresselhaus, G. Dresslhaus, Annu. Rev. Mater. Sci. **25**, 487 (1995)
16. H. Kataura, Y. Endo, Y. Achiba, K. Kikuchi, T. Hanyu, S. Yamaguchi, J. Phys. Chem. Solids **58**, 1913 (1997)
17. T. Gotoh, S. Nonomura, S. Hirata, S. Nitta, Appl. Surf. Sci. **113/114**, 278 (1997)
18. W. Zhou, S. Xie, S. Qian, T. Zhou, R. Zhao, G. Wang, L. Qian, W. Li, J. Appl. Phys. **104**, 459 (1996)

19. H. Habuchi, S. Nitta, D.X. Han, S. Nonomura, J. Appl. Phys. **87**, 8580 (2000)
20. A.D.Z. Mendaza, J. Bergqvist, O. Bäcke, C. Lindqvist, R. Kroon, F. Gao, M.R. Andersson, E. Olsson, O. Inganäs, C. Müller, J. Mater. Chem. A **2**, 14354–14359 (2014)
21. R. Von Hipple, *Dielectrics and Waves* (Wiley, New York, 1954)
22. M. Pollak, G.E. Pike, Phys. Rev. Lett. **28**, 1444 (1972)
23. K. Jonscher, Nature **267**, 673 (1977)
24. S.R. Elliott, Adv. Phys. **36**, 135 (1987)
25. S.M. Soosen, A. Chandran, J. Koshy, K.C. George, J. Appl. Phys. **109**, 113702 (2011)
26. C. Shen, A. Kahn, J. Schwartz, J. Appl. Phys. **89**, 449 (2001)
27. V.I. Arkhipov, P. Heremans, E.V. Emelianova, H. Bässler, Phys. Rev. B **71**, 045214 (2005)